Photosynth Res
DOI 10.1007/s11120-015-0162-5

REGULAR PAPER

Enhanced photocurrent from Photosystem I upon in vitro truncation of the antennae chlorophyll

J. Ridge Carter[1] · David R. Baker[2] · T. Austin Witt[1] · Barry D. Bruce[1,3]

Received: 30 January 2015 / Accepted: 22 May 2015

Abstract Current effects on climate change and dwindling fossil fuel reserves require new materials and methods to convert solar energy into a viable clean energy source. Recent progress in the direct conversion of light into photocurrent has been well documented using Photosystem I. In plants, PSI consists of a core complex and multiple light-harvesting complexes, denoted LHCI and LHCII. Most of the methods for isolating PSI from plants involve a selective, detergent solubilization from thylakoids followed by sucrose gradient density centrifugation. These processes isolate one variant of PSI with a specific ratio of Chl:P_{700}. In this study, we have developed a simple and potentially scalable method for isolating multiple PSI variants using Hydroxyapatite chromatography, which has been well documented in other Photosystem I isolation protocols. By varying the wash conditions, we show that it is possible to change the Chl:P_{700} ratios. These different PSI complexes were cast into a PSI–Nafion–osmium polymer film that enabled their photoactivity to be measured. Photocurrent increases nearly 400 % between highly washed and untreated solutions based on equal chlorophyll content. Importantly, the mild washing conditions remove peripheral Chl and some LHCI without inhibiting the photochemical activity of PSI as suggested by SDS-PAGE analysis. This result could indicate that more P_{700} could be loaded per surface area for biohybrid devices. Compared with other PSI isolations, this protocol also allows isolation of multiple PSI variants without loss of photochemical activity.

Keywords Photosystem I · Hydroxyapatite · Photocurrent · Chlorophyll · Light-harvesting complex I, II

Introduction

Sunlight is an attractive energy source to mitigate the increasing energy demands worldwide (Armaroli and Balzani 2006). Nature has harnessed this energy with the evolution of photosynthesis, specifically the light-dependent reactions. Electrons that are generated from the oxidation of water by Photosystem II (PSII) pass through a redox cascade involving several proteins and cofactors until reaching Photosystem I (PSI), which has the most reductive biological redox potential known (Nelson 2009). PSI is a protein complex that helps drive the light reactions in the thylakoid membrane. Light energy is transferred by peripheral chlorophyll (Chl) molecules and antenna proteins to the special pair Chl (P_{700}), or reaction center, where an electron–hole pair is generated. The photoexcited electron is transferred across the protein where it is used to reduce Ferredoxin and subsequently $NADP^+$. Isolated PSI has been employed in a wide range of applications from using proteoliposomes in order to photosensitize mammalian cells to suspending PSI particles in a Nafion film in solid-state photovoltaics (Baker et al. 2014b; Kuritz et al. 2005).

PSI has evolved from a trimer in cyanobacteria to a monomer in plants with a potential tetrameric intermediate

✉ Barry D. Bruce
bbruce@utk.edu

[1] Department of Biochemistry and Cellular and Molecular Biology, University of Tennessee, Knoxville, TN 37996, USA

[2] Sensors and Electron Devices Directorate, United States Army Research Laboratory, Adelphi, MD 20783, USA

[3] Program in Energy Science and Engineering, University of Tennessee, Knoxville, TN 37996, USA

Published online: 02 June 2015

(Fromme et al. 2001; Li et al. 2014). The resolution of the crystal structure for *P. sativum* PSI has recently been improved from 3.4 to 3.3 Å as shown in Fig. 1 (Amunts et al. 2007, 2010). Plant PSI is composed of the PSI core and antenna proteins, Light-Harvesting Complex I (LHCI) and transiently associated Light-Harvesting Complex II (LHCII). Historically, the plant PSI core contains 12 subunits, 10 of which are conserved with cyanobacterial PSI (Amunts et al. 2010); however, two recent studies have discovered PsaO and PsaP subunits involved in the interaction between the PSI core and antenna (Khrouchtchova et al. 2005; Knoetzel et al. 2002). The very similar, large subunits, PsaA and PsaB, house the special pair Chl that constitutes the P_{700} center (Amunts et al. 2007), which collects photon energy funneled to it by the Chl scattered throughout the rest of the PSI–LHC complex. In order to facilitate light harvesting in varying light conditions, green plants and algae have evolved two light-harvesting complexes, LHCI and LHCII (Allen et al. 1981; Amunts et al. 2010; Nelson and Ben-Shem 2005). Under intense light conditions, the light-harvesting complexes are not as crucial (Muller et al. 2001). In *P. sativum*, LHCII associates with the PsaH subunit on the stromal side and is only associated with PSI during state transitions of high light intensity, while LHCI is anchored around half of the PSI core via PsaG (Nelson and Ben-Shem 2005). Studies have indicated at least 4 LHCI monomers in higher plants (Lhca1, 2, 3, 4) (Haworth et al. 1983; Ikeuchi et al. 1991; Mullet et al. 1980), and the Lhca1 protein is the only monomer consistently seen under all light conditions (Nelson and Ben-Shem 2005). In some algae such as *Chlamydomonas reinhardtii*, however, studies have revealed that as many as nine Lhcas can associate with the PSI core

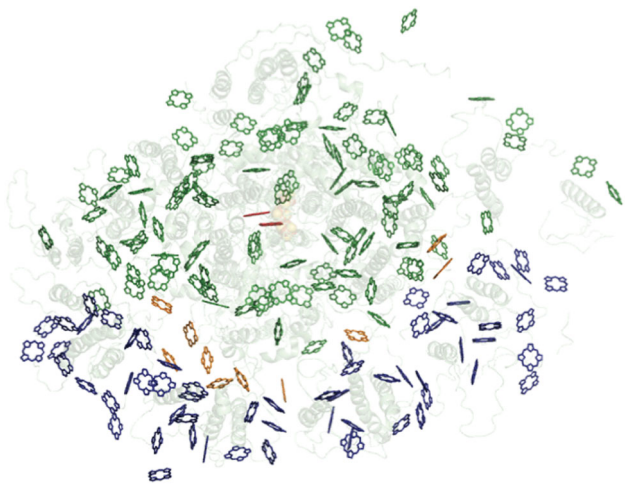

Fig. 1 Crystal structure of higher plant PSI (*Pisum sativum*). *Blue Chl* LHCI. *Orange Chl* "gap" Chl. *Green Chl* PSI core. *Red Chl* special pair reaction center P_{700}. PDB file 3LW5

complex in a double half-ring as opposed to the single half-ring seen in Fig. 1 (Drop et al. 2011). These antenna proteins can be detrimental to photosynthetic activity because LHCI has a much higher photon absorption rate than the PSI complex (Kirst et al. 2012), which is useful for low-light conditions, but in high-intensity environments the cell organism must eliminate excess absorbed photon energy by non-photochemical quenching to avoid damaging side effects, thereby negatively affecting the photochemical quantum efficiency in high-light conditions (Kirst et al. 2012). Several studies have attempted to maximize photosynthetic activity and avoid this shielding effect via genetic mutation of the antenna (Kirst et al. 2012; Melis 2009). For example, Kirst et al. showed that photosynthetic activity was increased upon deletion of the TLA3-CpSRP43 gene in *C. reinhardtii* which reduced the overall antenna size to approximately 40 % of WT (2012). The mutant even continued to show increased photosynthetic activity well beyond the saturation light intensity for WT ($\sim$500 μE $m^{-2}s^{-1}$) and even until full-sunlight levels ($\sim$2000 μE $m^{-2}s^{-1}$). These studies delineate the production of a finite PSI variant by genetic mutation, but a less-invasive method for isolating a range of PSI–LHC variants is detailed in this study. We define PSI variants as differences in Chl:P_{700} ratios based on size and pigment content. Although genetic mutation has allowed the isolation of a single PSI variant with a single Chl:P_{700} ratio, there is currently not a method for non-invasively isolating multiple PSI variants.

One previous method for isolation of PSI, hydroxyapatite (HA) chromatography, has the potential to be used on an industrial scale for the purpose of isolating multiple PSI variants as detailed in this study (Hiyama 2004; Lee et al. 1992; Shiozawa et al. 1974). HA is a natural multimodal medium consisting of calcium- and phosphate-binding sites, which interact by metal affinity and cation exchange, respectively (Gagnon 2010). A specific combination of type and size of particle is needed depending on the specific protein being purified. CHT™ I and II particles can adsorb >25 mg and between 12 and 19 mg, respectively, with the option of 20, 40, or 80 μm particle size (Cummings et al. 2009). Although HA has been previously used for PSI isolation, these studies did not use it for a gradient isolation of PSI variants (Lee et al. 1992; Shiozawa et al. 1974). A fine-tuned HA chromatography process allows the tailored isolation of PSI with a range of Chl:P_{700} ratios because the PSI may be isolated with varying degrees of truncation of the antenna proteins and removal of Chl. Moreover, this process is likely to maintain the functionality of the protein, which is important for use in the rapidly advancing field of PSI-based photovoltaics (Nguyen and Bruce 2014).

Materials and methods

Isolation of PSI

Preparation of spinach PSI was adapted from Bruce and Malkin (1988). Baby spinach leaves were purchased commercially, finely chopped in a food processor, and resuspended in grinding buffer (50 mM Hepes–KOH pH 7.3, 330 mM sorbitol, 0.1 % BSA, 5 mM $MgCl_2$, 5 mM $MnCl_2$, 2 mM Na_2EDTA) at approximately 2 ml grinding buffer per 1 g spinach leaves. The slurry was then gently homogenized with a Polytron® from Brinkmann Instruments for 10 s. The resulting slurry was rigorously squeezed through 2 layers of Miracloth (Calbiochem) and 2 layers of cheese cloth, respectively, until all the liquid had passed through the filters. The remaining cell debris was discarded, and the solution was pelleted at $4000\times g$ for 10 min. The supernatant was discarded while the pellet was resuspended in 150 mM NaCl. The solution was then pelleted at $12{,}000\times g$ for 10 min.

All of the following steps were conducted in the dark unless otherwise noted. The pellet was resuspended in 2 M NaBr to 0.8 mg/ml, incubated at 4 °C for 45 min, and pelleted at $12{,}000\times g$ for 10 min. The previous step was repeated. The subsequent pellet was resuspended in 50 mM sorbitol and 5 mM EDTA-NaOH pH 7.8 at 0.8 mg Chl/ml and pelleted at $12{,}000\times g$ for 10 min. The pellet was resuspended in ddH_2O, and the Chl concentration was measured again. The solution was then brought up to a final Chl concentration of 0.8 mg/ml and 1.2 % Anapoe X-100 (Triton X-100) from Anatrace. The solution was solubilized at room temperature for 1 h and then centrifuged at $40{,}000\times g$ for 30 min. The supernatant was loaded on a sucrose gradient.

A sucrose gradient was prepared and centrifuged according to Mullet et al. with the following modifications (Mullet et al. 1980). A 22 ml linear gradient (0.1–1.0 M) and 2 ml cushion (2 M) were prepared. After loading the supernatant on top of the gradient, it was centrifuged at $140{,}000\times g$ for 16 h. The bottom band was collected and stored at −80 °C for future use.

HA chromatography

This protocol was adapted from the work of Shiozawa et al. (1974) and Hiyama (2004) with some important differences. All buffers were prepared according to Bio-Rad instruction manual, Hiyama (2004) and Cummings et al. (2009). Glass Econo-Column® Chromatography Columns 2.5 × 10 cm and CHT Ceramic Hydroxyapatite Type II Support with a 40 μm particle size were purchased from Bio-Rad. The HA matrix was initially sanitized by mixing 10 g of HA matrix with 2 M NaOH and allowing the matrix to settle for 30–60 min. Mixing was conducted with a plastic spatula to avoid introducing metal ions to the matrix. The particles were then regenerated with 100 mM sodium phosphate buffer pH 8.0 via the same method as sanitization.

Unless otherwise noted, all chromatography was performed via gravity. The equilibration, wash, and elution volumes were calculated using column volumes (CV). In this study 1 CV = 20 ml. The matrix was mixed with 50 ml packing buffer (0.2 M sodium phosphate buffer pH 9–10) and gravity packed in the glass column. Without disturbing the column bed, the matrix was equilibrated with 5 CV of equilibration buffer (10 mM Tris-HCl pH 8.8, 0.3 mM $CaCl_2$, 0.05 % Anapoe X-100). The protein sample was then loaded on the column after dilution with equal volume of wash buffer (10 mM Tris-HCl pH 7.5, 0.6 mM $CaCl_2$, 0.05 % Anapoe X-100). The amount of protein loaded onto column varied but did not exceed the adsorption limits of the HA medium. The columns were washed with varying volumes (5–20 CV) of wash buffer, and the protein was then eluted with 2.5 CV elution buffer (100 mM sodium phosphate buffer pH 8.0, 0.05 % Anapoe X-100). The dark green band was collected from the eluate and stored in elution buffer at −80 °C until further characterization.

Transient photobleaching

Photobleaching of spinach PSI was conducted using a JTS-10 spectrometer from Bio-Logic. Spinach PSI samples were prepared in 1 ml total reaction volume with 2 μg Chl/ml, 2 mM sodium ascorbate, 1 mM methyl viologen dichloride (MV^{2+}), MES buffer pH 6.4, 0.03 % *n*-dodecyl-β-D-maltoside, and 10 molar excess *T. elongatus* (*T.e.*) cytochrome c_6.

Ambient light was subtracted before data collection. Individual samples were flashed with actinic light at 3000 μE $m^{-2}s^{-1}$ for 5 ms with a 705 nm cut-off filter. A non-actinic run was subtracted from the actinic flash for each sample. After the actinic flash, the change in the absorbance for 200 points was collected exponentially from 60 μs to 10 s, and fits were generated with GraphPad Prism® software.

Chlorophyll concentration

Chl concentrations were determined using a Shimadzu UV-160U spectrophotometer and according to Eq. 1 (Arnon 1949). For the absorbance measurements, 10 μl of sample was added to 990 μl of an 80 % acetone, 20 % ddH_2O solution.

$$\text{Chlorophyll}\left(\frac{\text{mg}}{\text{ml}}\right) = \frac{(8.02 \times A_{663}) + (20.2 \times A_{645})}{(\text{volume sample})\ \mu\text{l}} \quad (1)$$

Photocurrent

Electrode substrates were prepared by e-beam evaporation of 10 nm Ti onto indium-doped tin oxide (ITO)-coated glass slides (5–15 Ω, Delta Technologies Ltd.). This binding layer was subsequently coated with 300 nm of Au, also by e-beam evaporation. Electrodes were cut from the Au-coated slides into 2.5 × 0.8 cm chips. A 20 µl drop of a mixture containing 0.1 wt% Nafion, 32 µM $Os(bpy)_2Cl_2$, 47.5 mM Na-phosphate buffer pH 7, 0.024 wt% Triton, and PSI was dropped onto the Au electrode and allowed to air dry in the dark at room temperature (Baker et al. 2014b). PSI concentrations were adjusted between samples to maintain 1.9 µg Chl per electrode unless otherwise stated.

Photoelectrochemical measurements were performed using a 150 W Xe lamp (Newport Corporation), with an internal shutter, illuminating samples after the light was passed through a 676 nm bandpass filter (Edmund Optics). The power incident at electrode surfaces was 1.4 mW/cm^2 (~81 µE/m^2/s). Data were collected with a Gamry Reference 600 potentiostat in a 3-electrode arrangement with an Ag/AgCl 3 M KCl reference electrode and a Pt wire counter electrode. The aqueous electrolyte solution was 0.1 M $MgCl_2$ and 250 µM MV^{2+}. Samples were under an applied potential of −0.2 V versus Ag/AgCl, which was applied for 5 min before testing to equilibrate the system prior to the experiment, and this wait period also allows the Nafion film to fully hydrate (Baker et al. 2014b). Photocurrent measurements consisted of a 1-min illumination period followed by 2 min in the dark. After subtracting any transient background current, the difference between the current at the end of the illumination period and the end of the dark period was considered the photocurrent. Electrode areas varied slightly from sample to sample, but were approximately 0.25 cm^2.

Chl:P_{700} ratios were approximately determined from a JTS-10 to an absorbance conversion factor of 4.35 × 10^{-7} and a Chl A/B mass of 897 g mol^{-1}. The spinach P_{700} extinction coefficient of 64,000 L mol^{-1} cm^{-1} was obtained from Hiyama and Ke (1972).

SDS- and BN-PAGE

A 16 ml 12.5–20 % acrylamide linear gradient was prepared for the resolving layer using a Hoefer vertical unit from Harvard Apparatus. The 12.5 % acrylamide also had 4 % sucrose and 1X resolving gel buffer pH 8.3 (25 mM Tris, 0.1 % SDS, 275 mM glycine), and the 20 % acrylamide had 13 % sucrose and 1X resolving gel buffer. The remainder of the gel was capped off with stacking gel [4.8 % acrylamide, 1X stacking gel buffer (125 mM Tris pH 6.8, 0.1 % SDS)]. Samples were solubilized in sample solubilizing buffer (100 mM DTT, 10 mM Tris pH 6.8, 10 % glycerol, 1 % SDS, 0.01 % Bromophenol Blue) at 30 °C for 1 h. A Mark 12™ Unstained Standard from Life Technologies™ was used as a protein molecular marker. The gel was run at 6 mA constant for 14 h in SDS-running buffer (0.03 % Tris (pH to 8.3–8.4 with glycine), 0.01 % SDS). The gel was then stained for 1 h (50 % methanol, 10 % acetic acid, 0.1 % R-250 Coomassie Brilliant Blue) and subsequently destained overnight (40 % methanol, 5 % acetic acid).

The BN-PAGE gel analysis was performed according to the protocol from Invitrogen, and the NativeMark™ standard was also obtained from Invitrogen. The 1068 kDa PSI trimer standard was obtained from Li et al. (2014). The destain solution was the same as for SDS except that it was diluted with approximately 0.5–1X H_2O.

Histogram

A histogram of each lane was obtained using Quantity One® software from Bio-Rad. Peaks were aligned by adjusting the lane length. The background was removed from each lane using the rolling ball function.

Results and discussion

SDS-PAGE

HA chromatography columns (6 columns processed in parallel) were packed with approximately 20 ml bed volume of HA medium. Post sucrose gradient samples (0 CV) were then loaded onto the columns. Samples were first purified via sucrose so that less contaminant was introduced to the column. Less contamination allowed easier characterization of elution products; however, preliminary work showed that pure samples could potentially be obtained without the use of sucrose gradients. Then, each sample was washed with a different volume of wash buffer, which contained Triton X-100. The wash buffer stripped away peripheral Chl and antenna subunits to varying degrees, allowing isolation of multiple PSI variants. The isolation of a range of PSI variants differed from the protocols discussed in Lee et al. (1992) and Shiozawa et al. (1974). After elution with phosphate buffer, fractions were collected, concentrated, and run over a Tris-glycine SDS-PAGE with a linear acrylamide gradient from 12.5 to 20 % as seen in Fig. 2. The sizes of the prominent PSI core subunits (PsaA/B, PsaC, PsaD, PsaE, PsaF, PsaH) for

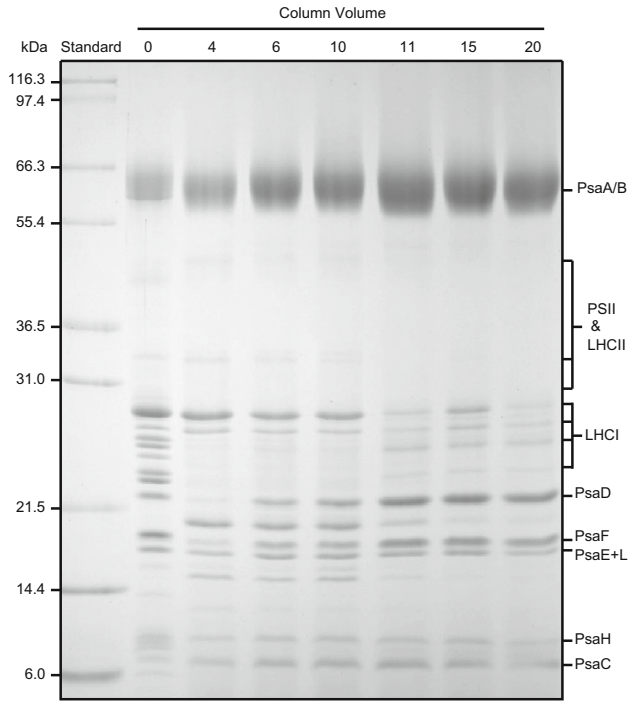

Fig. 2 SDS-PAGE of spinach PSI samples with varying wash volumes. Each *lane* was loaded with 4.8 μg Chl. 1 CV = 20 ml of wash buffer. Tris-glycine gel with 12.5–20 % acrylamide. Mark 12™ protein standard from Invitrogen

higher plants were in agreement with previous studies (Bruce and Malkin 1988; Mullet et al. 1980; Zilber and Malkin 1992). As evidenced by the gel, which was loaded on an equal Chl basis, the antenna subunits and other contaminants were gradually stripped away as the PSI core became more purified with increasing wash volume. By 20 CV, all the PSII and LHCII contaminant had been removed, indicating that the two-step purification process of HA chromatography plus ultracentrifugation provided a purer product than ultracentrifugation alone. Although most of LHCI had been stripped from the PSI core after 20 CV, it had not been completely removed.

It was also possible that the LHCI had been detached from PSI only to reattach to the HA medium. For example, an LHCI subunit could have been stripped from the PSI core only to rebind to the HA medium, which would then have eluted from the column along with the PSI core. Furthermore, an SDS-PAGE gel could not differentiate whether the LHCI subunit is still attached to the PSI core. The gel did show that the ratio of LHCI subunits to PSI core subunits decreased with increasing wash volume.

Consequently, one caveat to using HA chromatography is that it is not specific to PSI. Therefore, it was possible to have degradation products reattach to the column. There are several that appeared in later washes that are not present in the initial starting material (0 CV). This disparity could have been attributed to degradation products of higher molecular weight subunits, possibly due the presence of detergent, Triton X-100, in the wash buffer.

The dramatic shift between 0 and 20 CV is further shown by histogram analysis in Fig. 3. The histogram showed that the ratio of PSI core subunits to total protein is increasing with increasing wash volume as the ratio of PSII, LHCII, and LHCI subunits to total protein is decreasing.

Transient photobleaching

Using a JTS-10 spectrometer, P_{700} photobleaching was determined for PSI samples that were washed with varying volumes of wash buffer. Figure 4 shows the average amplitudes of photobleaching, which were obtained by averaging the largest amplitude values between 0 and 1 s after the actinic flash. For convenience sake, the values have been made positive. These values indicate a relative value of active P_{700} reaction centers in each sample because a 705 nm filter was used between the actinic flash and sample.

It proved to be exceedingly difficult to repeat column packing between each run. In addition, six columns were run simultaneously in order to increase efficiency. Therefore, although much effort was put forth to replicate the packing procedure between each column, slight variances could not be avoided. Some earlier runs showed that columns packed with detergent gave more homogenous samples with little variance when increasing wash volume (data not shown).

Photocurrent

Although methods have been developed to measure the photocurrent of an individual PSI molecule, ~10pA (Gerster et al. 2012), photocurrent was obtained using a Nafion film dried with a redox mediator and PSI embedded in the film as depicted in Fig. 5. Figure 6A shows a plot of chronoamperometric behavior for one light/dark cycle, and it is also clear that the Nafion–Os polymer had negligible inherent photoactivity. More extensive chronoamperometric data show that the 0 CV sample has a reduction of photocurrent over multiple light/dark cycles (data not shown). This decay was mostly attributed to the films falling off the electrode rather than Chl degradation. Photocurrent values were plotted against the corresponding wash volumes as shown in Fig. 6b. It appears that photocurrent plateaus at 1.75 μA cm^{-2}, after a nearly 400 % increase from 0.43 μA cm^{-2} at 0 CV, producing a current density of 1.25 μA cm^{-2} mW^{-1} when normalized for an incident illumination of 1.4 mW cm^{-2}. In comparison, other studies, such as Gunther et al. (2013), Ciesielski et al.

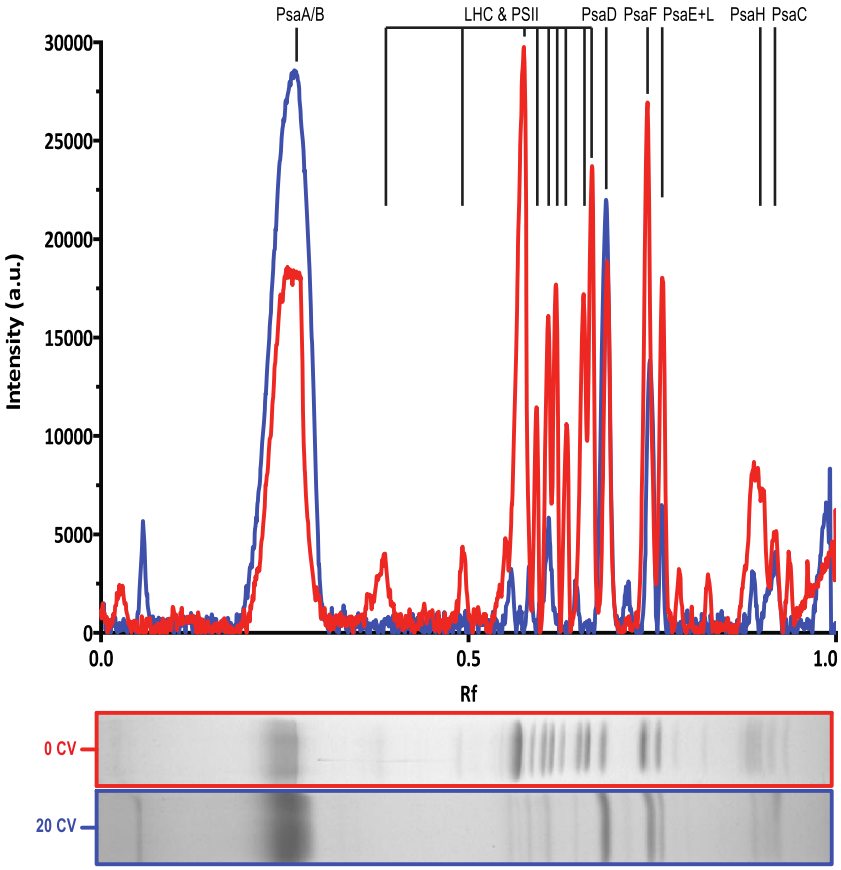

Fig. 3 Histogram analysis of *lanes* 2 (0 CV) and 8 (20 CV) from Fig. 1. Select peaks are labeled with corresponding subunit. *Red* denotes 0 CV. *Blue* denotes 20 CV. Analysis performed with Quantity One® software from Bio-Rad

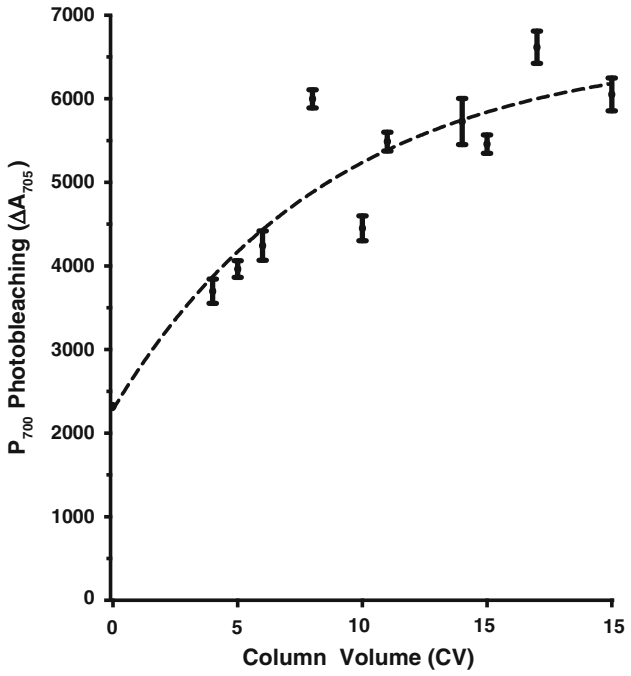

Fig. 4 P_{700} photobleaching of spinach PSI samples washed with increasing volume of wash buffer. Each sample contained 2 µg/ml Chl. *Error bars* represent standard error. One-phase decay fit was generated in GraphPad Prism 6. $R^2 = 0.84$

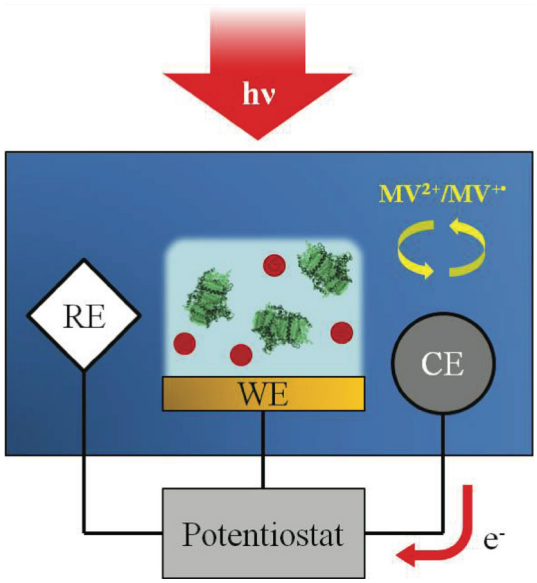

Fig. 5 Photoelectrochemical schematic depicts the potentiostat controlling the Ag/AgCl reference electrode (RE), the Pt wire counter electrode (CE), and the working electrode (WE) composed of the Au back electrode coated with the PSI/$Os(bpy)_2Cl_2$/Nafion film mixture inside the electrochemical cell with an electrolyte of 250 µM MV^{2+} and 0.1 M $MgCl_2$

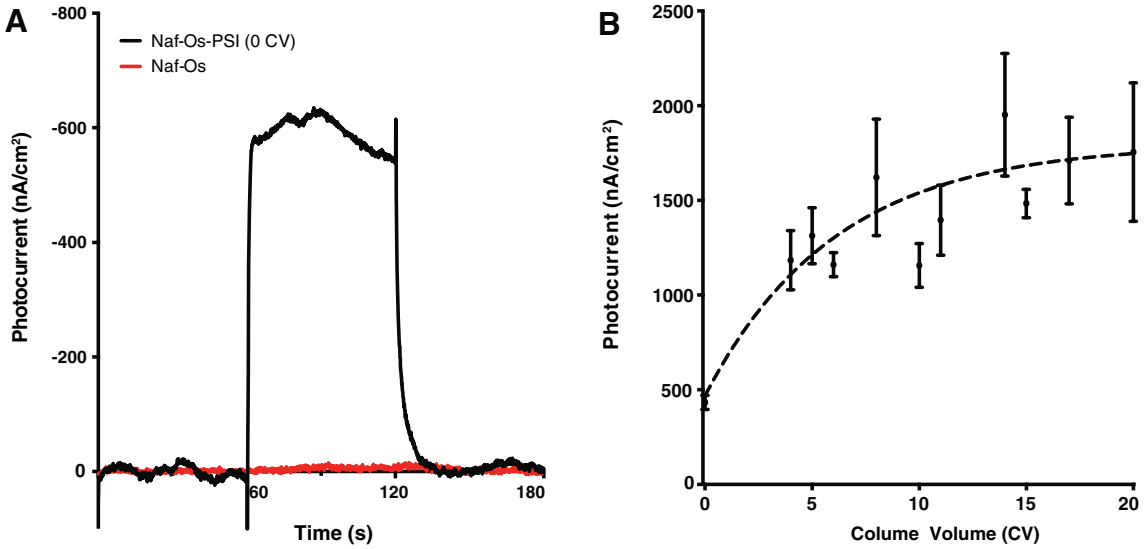

Fig. 6 **a** Photocurrent measurements of Nafion–Os–PSI film with (*black*) and without (*red*) PSI. PSI with no HA treatment (0 CV) was used. Incident illumination was 1.4 mW/cm^2 at 676 nm light with a 1-min on/off cycle. **b** Photocurrent of spinach PSI samples in a Nafion cell. Column volume represents volume of wash buffer used during HA chromatography. Each sample contained 5.7 μg Chl/electrode. *Error bars* represent standard error. One-phase decay fit and standard error was generated in GraphPad Prism 6. $R^2 = 0.78$

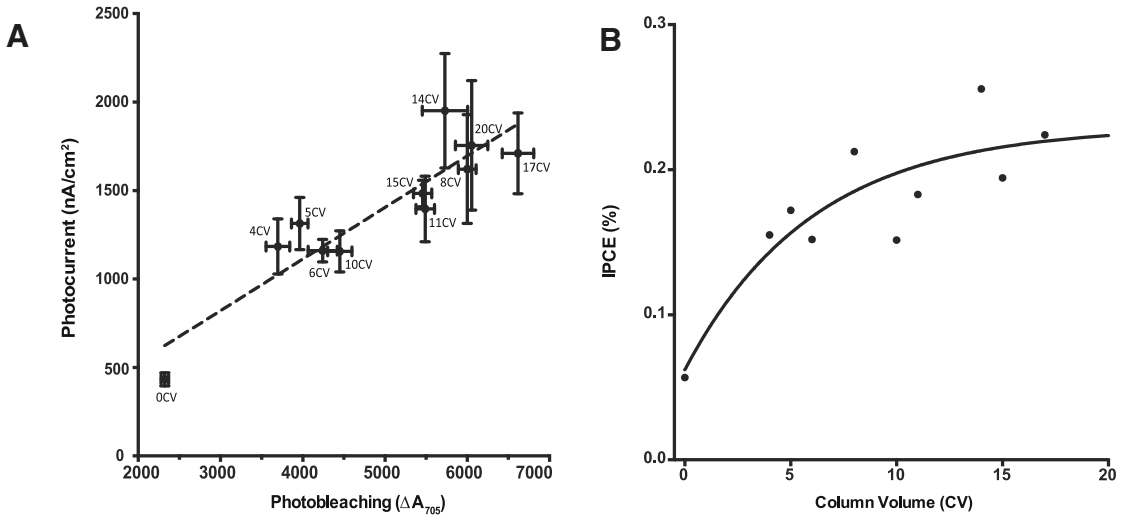

Fig. 7 **a** Column volume denotes volume of wash buffer used during HA chromatography. *Error bars* represent standard error. Linear regression and standard were generated in GraphPad Prism 6 and Microsoft® Excel. $R^2 = 0.83$. **b** Incident photon to charge carrier efficiency with an incident illumination of 1.4 mW/cm^2 at 676 nm light for various Chl concentrations per reaction center. All samples contained 1.9 μg Chl. One-phase decay fit was generated in GraphPad Prism 6. $R^2 = 0.78$

(2010b), Ciesielski et al. (2008, 2010a), and LeBlanc et al. (2012), have used spinach PSI in biohybrid devices and produced 0.0056, 0.083, 0.081, 0.14, and 4.6 μA cm^{-2} - mW^{-1} current densities, respectively, when normalized for incident illumination.

The variance of measured photocurrent within each individual sample could be attributed to the inherently heterogeneous nature of the drying process when forming the Nafion–PSI films. Slight changes in the PSI density across the film can cause variability in how much light is absorbed and the efficiency of transferring electrons from PSI reaction centers to the Au substrate. One of the major limiting factors for the photobleaching and photocurrent measurements is the number of available, active reaction centers. When Chl and antenna subunits were stripped from the PSI complex by wash buffer during HA chromatography, there were more reaction centers on a per Chl basis; however, it was important to demonstrate that truncation of the PSI–LHC complex did not inhibit the photochemical activity of the individual complexes. Consequently,

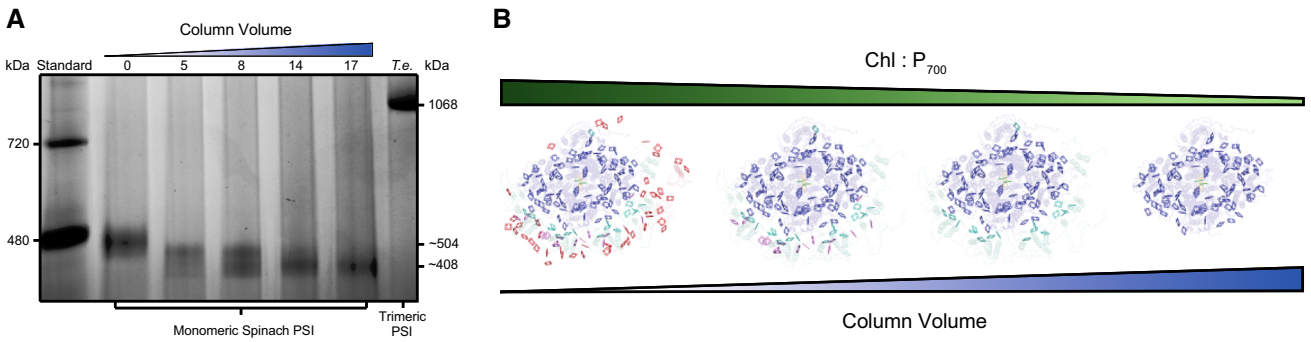

Fig. 8 **a** BN-PAGE of spinach PSI isolated via HA chromatography using 4–16 % BN-PAGE gel and NativeMark™ standard from Invitrogen. The approximate kDa values on the right determined from Rf calculations using the NativeMark™ standard values as well as the known molecular weight (1068 kDa) of *T.e.* PSI trimer. *Lanes* 2–7 loaded with 0.2 μg Chl. The 0 CV sample is representative of a standard sucrose density centrifugation isolation of higher plant PSI. **b** Proposed artistic model of higher plant PSI variants upon truncation via HA chromatography with increasing column volume of wash buffer (10 mM Tris-HCl pH 7.5, 0.6 mM $CaCl_2$, 0.05 % Triton X-100) applied to matrix. *Chl colors* represent truncation steps. Created from PDB file 3LW5

photocurrent was plotted against photobleaching as shown in Fig. 7a. A linear relationship between photocurrent and photobleaching was observed, indicating that photocurrent proportionally increases to the number of P_{700} reaction centers. These data also support the assertion that the removal of the peripheral Chl and truncation of the antenna during the HA isolation process were not detrimental to the ability of the protein to produce photocurrent. The incident photon to charge carrier efficiency (IPCE) at 676 nm is shown in Fig. 7b.

An inverse relationship between wash volume and size of monomeric spinach PSI can be seen in the BN-PAGE gel in Fig. 8a. The size of the monomeric spinach PSI decreased as wash volume increased. From the representative 0 CV to the 17 CV sample, a size shift of approximately 100 kDa was determined with a linear regression in Excel generated using the NativeMark™ and known *T.e.* trimer standards. The smearing of the monomeric PSI bands was likely caused by the existence of mixed PSI species. It appears that the monomeric bands became tighter with increasing wash volume, which indicates an increasingly homogenous isolation of PSI variant. In order to better visualize this gradient isolation of PSI variants and truncation of Chl and antenna subunits of higher plant PSI, an artistic model can be seen in Fig. 8b. Only the porphyrin ring of the Chl is shown. Each color represents a "truncation" variant. For example, the red Chl and subunits represent the first major truncation, magenta the second, cyan the third, and blue the final variant. As evident by the figure, it is proposed that the biggest elimination of Chl along with peripheral subunits occurs in the initial column volumes. It is also proposed that most of the LHCI subunits begin to detach from the PSI core from 8 to 20+ CV of wash buffer. Intermediate variants are not shown for ease of viewing.

Conclusions and future direction

Using HA chromatography to further isolate higher plant PSI after sucrose density centrifugation, we were able to increase photocurrent by approximately 400 % on a per Chl basis, which is a substantial increase. Furthermore, when the photocurrent is normalized for incident illumination, this system has a photocurrent of 1.25 μA cm^{-2} - mW^{-1} at 20 CV, which is an improvement on many other systems that use spinach PSI (Gunther et al. 2013; Ciesielski et al. 2010b; Ciesielski et al. 2008, 2010a), and only one study was found to be better (LeBlanc et al. 2012). In this study, variants can be isolated to tailor to the researcher's need. For instance, in low-light conditions, a researcher might need a PSI variant closer to the second and third variants in Fig. 8b to maximize light harvesting. Alternatively, a researcher might need a variant closer to last variant in Fig. 8b for high-light conditions or for dense packing of PSI. Moreover, Fig. 7 indicates that the isolation process does not inhibit photoactivity or IPCE of the P_{700} reaction centers, and Fig. 8a shows a 100 kDa size reduction. Thus, researchers such as Ciesielski et al. (2010a) that use dense layers of PSI on biohybrid devices to generate photocurrent would be able to pack more PSI onto the device without compromising photochemical activity by isolating PSI using our method. Consequently, more photocurrent would be generated in a given surface area. In relation, other studies have demonstrated that cyanobacterial PSI, which has a predominately trimeric PSI, does not lose photoactivity when broken into monomers and could thus also facilitate tighter packing of PSI in biohybrid devices without loss of photoactivity (Baker et al. 2014a).

Another benefit to truncating the light-harvesting complexes is that the shielding effect would be diminished as

discussed previously. It is important to note that the shielding effect is especially augmented with dense solutions of PSI–LHC complexes. Consequently, the thin layer of PSI–LHC used in this study to obtain photocurrent measurements would be less susceptible to dissipation of light energy as heat because of the superficial layer of PSI. However, other biohybrid devices employ dense layers of PSI and could thus benefit from truncating the peripheral LHC to reduce the shielding effect.

The ability to isolate multiple PSI–LHC variants is unique to the HA chromatography method as opposed to the singular variants created by ultracentrifugation, HPLC, and genetic mutation. Furthermore, the HA isolation process has the ability to find a photocurrent "sweet spot" by gradually increasing the wash volume to isolate the ideal variant mixture for the given application. Additional studies are needed to verify if the photocurrent versus photobleaching data maintain a linear relationship upon increasing wash volume or if the increased wash becomes detrimental to the photoactivity of the PSI complex.

Lastly, HA chromatography has the potential to be used on a much larger industrial scale as compared to ultracentrifugation and is less invasive than genetic mutation. Ultracentrifugation is a time- and labor-intensive step during PSI isolation for higher plants, and it can only process a small volume of sample (<50 ml per ultracentrifuge per 12–16 h). HA chromatography, on the other hand, could completely eliminate this overnight step in the future and also process exponentially more samples due to the abundance of HA, mechanical packing, and pumping. Preliminary work already suggests that this industrial process could be possible (data not shown), but further work is still needed.

Acknowledgments We would like to thank the Army Research Laboratories (ARL Contract #W91 1NF-11-2-0029), TN-SCORE sponsored by NSF-EPSCoR (EPS-1004083), and the Gibson Family Foundation for the generous funding for this project. We also appreciate the support and feedback provided by Khoa Nguyen, Prakitchai Chotewutmontri, and Richard Simmerman, and Ed Wright while conducting this research.

References

Allen JF, Bennett J, Steinback KE, Arntzen CJ (1981) Chloroplast protein phosphorylation couples plastoquinone redox state to distribution of excitation energy between photosystems. Nature 291:25–29

Amunts A, Drory O, Nelson N (2007) The structure of a plant Photosystem I supercomplex at 3.4 Å resolution. Nature 447:58–63. doi:10.1038/nature05687

Amunts A, Toporik H, Borovikova A, Nelson N (2010) Structure determination and improved model of plant Photosystem I. J Biol Chem 285:3478–3486. doi:10.1074/jbc.M109.072645

Armaroli N, Balzani V (2006) The future of energy supply: challenges and opportunities. Angew Chemi Int Ed 45:2–17

Arnon DI (1949) Copper enzymes in isolated chloroplasts. Polyphenoloxidase in *Beta vulgaris*. Plant Physiol 24:1–15

Baker DR et al (2014a) Comparative photoactivity and stability of isolated cyanobacterial monomeric and trimeric Photosystem I. J Phys Chem B 118:2703–2711. doi:10.1021/jp407948p

Baker DR, Simmerman RF, Sumner JJ, Bruce BD, Lundgren CA (2014b) Photoelectrochemistry of Photosystem I bound in nafion. Langmuir. doi:10.1021/la503132h

Bruce BD, Malkin R (1988) Subunit stoichiometry of the chloroplast Photosystem I complex. J Biol Chem 263:7302–7308

Ciesielski PN, Scott AM, Faulkner CJ, Berron BJ, Cliffel DE, Jennings GK (2008) Functionalized nanoporous gold leaf electrode films for the immobilization of Photosystem I. ACS Nano 2:2465–2472. doi:10.1021/nn800389k

Ciesielski PN et al (2010a) Photosystem I: based biohybrid photoelectrochemical cells. Bioresour Technol 101:3047–3053. doi:10.1016/j.biortech.2009.12.045

Ciesielski PN, Faulkner CJ, Iwin JM, Gregory JM, Tolk NH, Cliffel DE, Jennings GK (2010b) Enhanced photocurrent by Photosystem I multilayer assemblies. Adv Funct Mater 20:4048–4054. doi:10.1002/adfm.201001193

Cummings LJ, Snyder MA, Brisack K (2009) Protein chromatography on hydroxyapatite columns. Methods Enzymol 463:387–404. doi:10.1016/S0076-6879(09)63024-X

Drop B, Webber-Birungi M, Fusetti F, Kouril R, Redding KE, Boekema EJ, Croce R (2011) Photosystem I of Chlamydomonas reinhardtii contains nine light-harvesting complexes (Lhca) located on one side of the core. J Biol Chem 286:44878–44887. doi:10.1074/jbc.M111.301101

Fromme P, Jordan P, Krauss N (2001) Structure of Photosystem I. Biochim Biophys Acta 1507:5–31. doi:10.1016/S0005-2728(01)00195-5

Gagnon P (2010) Hydroxyapatite for biomolecule purification. Genet Eng and Biotechnol News 30(7):28

Gerster D et al (2012) Photocurrent of a single photosynthetic protein. Nat Nanotechnol 7:673–676. doi:10.1038/nnano.2012.165

Gunther D, LeBlanc G, Praisi D, Zhang JR, Cliffel DE, Bolotin KI, Jennings GK (2013) Photosystem I on graphene as a highly transparent, photoactive electrode. Langmuir 29:4177–4180. doi:10.1021/la305020c

Haworth P, Watson JL, Arntzen CJ (1983) The detection, isolation and characterization of a light-harvesting complex which is specifically associated with Photosystem I. Biochim Biophys Acta 724:151–158

Hiyama T (2004) Isolation of Photosystem I particles from spinach. Methods Mol Biol 274:11–17. doi:10.1385/1-59259-799-8:011

Hiyama T, Ke B (1972) Difference spectra and extinction coefficients of P700. Biochim Biophys Acta 267:160–171. doi:10.1016/0005-2728(72)90147-8

Ikeuchi M, Hirano A, Inoue Y (1991) Correspondence of apoproteins of light-harvesting chlorophyll *a/b* complexes associated with Photosystem I to cab genes: evidence for a novel type IV apoprotein. Plant Cell Physiol 32:103–112

Khrouchtchova A et al (2005) A previously found thylakoid membrane protein of 14 kDa (TMP14) is a novel subunit of plant Photosystem I and is designated PSI-P. FEBS Lett 579:4808–4812

Kirst H, Garcia-Cerdan JG, Zurbriggen A, Ruehle T, Melis A (2012) Truncated Photosystem chlorophyll antenna size in the green microalga *Chlamydomonas reinhardtii* upon deletion of the TLA3-CpSRP43 gene. Plant Physiol 160:2251–2260. doi:10.1104/pp.112.206672

Knoetzel J, Mant A, Haldrup A, Jensen PE, Scheller HV (2002) PSI-O, a new 10-kDa subunit of eukaryotic Photosystem I. FEBS Lett 510:145–148

Kuritz T, Lee I, Owens ET, Humayun M, Greenbaum E (2005) Molecular photovoltaics and the photoactivation of mammalian cells. IEEE Trans Nanobiosci 4:196–200

LeBlanc G, Chen G, Gizzie EA, Jennings GK, Cliffel DE (2012) Enhanced photocurrents of Photosystem I films on p-doped silicon. Adv Mater 24:5959–5962. doi:10.1002/adma.201202794

Lee JW, Zipfel W, Owens TG (1992) Quenching of chlorophyll excited states in Photosystem I by quinones: Stern–Volmer analysis of fluorescence and photochemical yield. J Lumin 51:79–89

Li M, Semchonok DA, Boekema EJ, Bruce BD (2014) Characterization and evolution of tetrameric Photosystem I from the thermophilic cyanobacterium *Chroococcidiopsis* sp. TS-821. Plant Cell. doi:10.1105/tpc.113.120782

Melis A (2009) Solar energy conversion efficiencies in photosynthesis: minimizing the chlorophyll antennae to maximize efficiency. Plant Sci 177:272–280. doi:10.1016/j.plantsci.2009.06.005

Muller P, Li XP, Niyogi KK (2001) Non-photochemical quenching. A response to excess light energy. Plant Physiol 125:1558–1566

Mullet JE, Burke JJ, Arntzen CJ (1980) Chlorophyll proteins of Photosystem I. Plant Physiol 65:814–822

Nelson N (2009) Plant photosystem I—the most efficient nano-photochemical machine. J Nanosci Nanotechnol 9:1709–1713

Nelson N, Ben-Shem A (2005) The structure of Photosystem I and evolution of photosynthesis. BioEssays 27:914–922. doi:10.1002/bies.20278

Nguyen K, Bruce BD (2014) Growing green electricity: progress and strategies for use of Photosystem I for sustainable photovoltaic energy conversion. Biochim Biophys Acta. doi:10.1016/j.bbabio.2013.12.013

Shiozawa JA, Alberte RS, Thornber JP (1974) The P700-chlorophyll a-protein. Isolation and some characteristics of the complex in higher plants. Arch Biochem Biophys 165:388–397

Zilber AL, Malkin R (1992) Organization and topology of Photosystem I subunits. Plant Physiol 99:901–911